Nanoscale

PAPER

View Article Online
View Journal | View Issue

Cite this: *Nanoscale*, 2015, **7**, 1333

Broadband slow light in one-dimensional logically combined photonic crystals†

G. Alagappan* and C. E. Png

Received 3rd October 2014,
Accepted 24th November 2014

DOI: 10.1039/c4nr05810k

www.rsc.org/nanoscale

Here, we demonstrate the broadband slow light effects in a new family of one dimensional photonic crystals, which are obtained by logically combining two photonic crystals of slightly different periods. The logical combination slowly destroys the original translational symmetries of the individual photonic crystals. Consequently, the Bloch modes of the individual photonic crystals with different wavevectors couple with each other, creating a vast number of slow modes. Specifically, we describe a photonic crystal architecture that results from a logical "OR" mixture of two one dimensional photonic crystals with a periods ratio of $r = R/(R-1)$, where $R > 2$ is an integer. Such a logically combined architecture, exhibits a broad region of frequencies in which a dense number of slow modes with varnishing group velocities, appear naturally as Bloch modes.

Structures that are capable of slowing light in a broad range of frequencies are very useful in creating various slow light devices for optical communications.[1–3] Broadband slow light effects have been demonstrated in various optical systems. These include adiabatically graded metallic gratings,[4–6] flat band photonic crystal (PC) waveguides,[7–10] coupled periodic nanowires,[11] chirped hyperbolic metamaterials,[12] and metamaterials with double-continuum Fano resonance.[13] Most of these proposed structures involve geometries in two and three dimensions. It would be useful if one could implement broadband slow light effects in one-dimensional (1D) systems, where the fabrication feasibility is very high. Here, we show broadband light effects in a simple 1D system that has a dual periodicity. Although, 1D dual periodic structures have been analysed,[14–16] the potential broadband slow light behaviour of such systems was not shown. The dual periodic systems analysed previously were created by sinusoidally modulating the dielectric constant values of perfect 1D PCs. The small depth of dielectric modulation in such a system hinders the creation of multiple slow modes.

In this article, we demonstrate a novel technique of creating a dual periodic structure that has a huge refractive index contrast, and is capable of showing broadband slow light effects. Particularly, we introduce the idea of logical combination of PCs, in which the result of the combination delivers a logically combined PC, which is a form of a dual periodic structure. The new 1D architecture requires only two materials, and it is easy to implement either as a multilayer system, or using planar nano-lithographical techniques.

A dual periodic structure can be created, by periodically and slowly chirping the dielectric profile of an optical periodic structure [that has a fast changing dielectric profile]. This process is equivalent to the mixing of two periodic structures with almost the same periodicities. Two closely spaced periods are the basis for the "beat" effects occurring in the longer spatial scale. The mixing can be simply done by adding or averaging the two periodic dielectric functions. However, the resulting dielectric function may not be feasible for fabrication. For example, take a binary 1D PC constructed with alternating materials of dielectric constants of ε_a and ε_b. The addition of the dielectric functions of two such 1D PCs (with different periods) would result in a new dielectric profile with dielectric constant values ε_a, ε_b and $0.5(\varepsilon_a + \varepsilon_b)$ [after dividing by two]. This new dielectric profile requires a third material with a dielectric constant, $0.5(\varepsilon_a + \varepsilon_b)$, and evidently, this imposes a tough constraint on the implementation of the addition of PCs. Therefore, we seek the method of logical combination of PCs, in which the result of the combination retains the binary values ε_a and ε_b, and at the same time exhibits a similar spatial Fourier decomposition as that of an addition process.

Consider two 1D PCs, PC1 and PC2 with periods a and ra $(r > 1)$, respectively. Assume these two PCs are constructed with a pair of dielectric materials with dielectric constants, ε_a and ε_b. We can combine the dielectric functions of the two PCs, $\varepsilon_1(x)$ and $\varepsilon_2(x)$, using a logical operation at every point along the x-axis to generate a new dielectric function, $\varepsilon(x)$. For the purpose of illustration, in this article we will use a logical

Department of Electronics and Photonics, Institute of High Performance Computing, Agency for Science, Technology, and Research (A-STAR), Fusionopolis, 1 Fusionopolis Way, #16-16 Connexis, Singapore 138632. E-mail: gandhi@ihpc.a-star.edu.sg

†Electronic supplementary information (ESI) available. See DOI: 10.1039/c4nr05810k

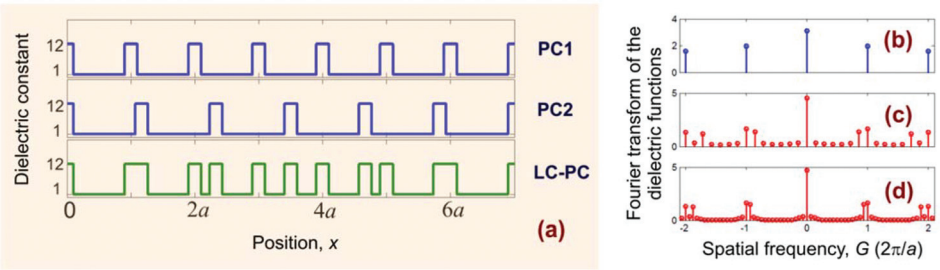

Fig. 1 (a) Dielectric functions of PC1, PC2, and the LCPC. Fourier transforms of the dielectric functions. (b) PC1; (c) LCPC with $R = 7$; (d) LCPC with $R = 16$.

"OR" operation to generate $\varepsilon(x)$. The logical "OR" operation will result in $\varepsilon(x)$ of ε_a, when $\varepsilon_1(x) = \varepsilon_2(x) = \varepsilon_a$. When $\varepsilon_1(x) = \varepsilon_2(x) = \varepsilon_b$ or $\varepsilon_1(x) \neq \varepsilon_2(x)$, the operation will give $\varepsilon(x)$ of ε_b. In this procedure, ε_b and ε_a are treated similar to the logical values of 0 and 1, respectively. If r is a rational number, then $\varepsilon(x)$ is periodic with a period, $a_s = Ra$, where R is the least integer multiple of r. The new 1D structure with a periodic $\varepsilon(x)$ is defined as a logically combined photonic crystal (LCPC).

In order to have a small value of r, we choose a system where in one period of the combined PC, we have R periods of PC1, and $R - 1$ periods of PC2. This will result in an LCPC of $a_s = Ra = (R - 1)ra$, with $r = R/(R - 1)$. Fig. 1(a) illustrates the logical combination of $\varepsilon_1(x)$ and $\varepsilon_2(x)$, for $R = 7$, $\varepsilon_a = 12$ [silicon], and $\varepsilon_b = 1$ [air]. The thicknesses of the silicon slabs in PC1 and PC2 are taken as $d = 0.2a$. As we have shown in the figure, the logical combination of R and $R - 1$ primitive unit cells of PC1 and PC2, produces one primitive unit cell of the LCPC. The primitive unit cell of the LCPC shown in Fig. 1(a), will repeat itself with the period a_s. The geometries of all LCPCs with $r = R/(R - 1)$, obtained *via* the logical "OR" operations can be described exactly. The number of silicon slabs in one period of the LCPC is $2R - 2n_c$, where n_c is the integral ceiling of $d/[a(r - 1)]$. If we take the floating point value for n_c, then the filling ratio, F, can be shown to be exactly $F = 2f - f^2/r - f/R$, where $f = d/a$ is the filling ratio of PC1. There are two important limits of r, that are worth mentioning.

• In the limit of $r \to \infty$ (or equivalently $R = 1$), the period of PC2 is infinitely larger than the period of PC1. Thus in this case, the logical "OR" combination of PC1 and PC2, produces PC1. The filling ratio in this limit reduces to $F = f$.

• In the limit of $r \to 1$, the corresponding LCPC does not reduce to PC1, but to an LCPC with $F = 2f - f^2$. Note that, $r = R/(R - 1)$ only approaches one and will never equal one for any value of R. When $r \to 1$, $R = r/(r - 1)$ is a huge integer. Therefore, the period of the super cell, $a_s = Ra$, becomes large, and the LCPC in this limit will support a large number of slow modes.

In the reciprocal space, the length of the primitive reciprocal lattice vector for the LCPC is $g = \frac{2\pi}{a_s} = \frac{2\pi}{Ra}$, which is R times shorter than the length of the primitive reciprocal lattice vector for the original PC [*i.e.*, PC1] which is $Rg = \frac{2\pi}{a}$. The Brillouin zone (BZ) for wavevectors (k) in the LCPC is $-\frac{\pi}{Ra} < k < \frac{\pi}{Ra}$, and it is R times smaller than the BZ of PC1, $-\frac{\pi}{a} < k < \frac{\pi}{a}$. Fig. 1(b) and (c) show the Fourier transforms of the dielectric functions of PC1 and LCPC, respectively. From Fig. 1(c), we can clearly see that LCPC has a strong mixture of two closely spaced spatial frequencies: $Rg = \frac{2\pi}{a}$, and $(R-1)g = \frac{2\pi}{ra}$. The spatial frequency decomposition remains similar for all higher values of R. As an additional example, the spatial Fourier decomposition for an LCPC with $R = 16$ is shown in Fig. 1(d).

Fig. 2(a) and (c) show the band structures[17] of PC1 and LCPC ($R = 7$), respectively, for wavevectors within their first BZs. Fig. 2(d) shows the transmission spectrum of the LCPC calculated using a transfer matrix method,[18] for four unit cells of the LCPC, assuming a vacuum ambience. The vertical axes in all these figures represent the normalized frequency, $\Omega = \frac{\omega a}{2\pi c}$, where ω and c are the angular frequency, and the vacuum speed of light, respectively. The calculated transmission spectrum for the LCPC [Fig. 2(d)] is in very good agreement with the calculated band structure [Fig. 2(c)]. From Fig. 2(c), we can see that the band structure of the LCPC exhibits many flat bands. Flat bands have small group velocities, and they are the signatures of slow modes. In the transmission spectrum, flat bands emerge as sharp resonant peaks [Fig. 2(d)]. Note that, as a consequence of the band folding in 1D PC,[17] the bands can be either positive or negatively sloped (*i.e.*, positive and negative group velocities). Positive and negative small group velocities indicate the propagation directions of the waves slowly moving forward and backwards, respectively.[10] The negative group velocity in 1D PC made of linear dielectric materials does not correspond to a fast light.[19,20] This is different from a negative group velocity experienced by the light with a positive phase index, near an atomic resonance in a nonlinear medium, which can indicate a fast light.[21]

Fig. 3(a) shows a series of band structures for LCPCs with R ranging from 7 to 51. As we can see from this figure, the band

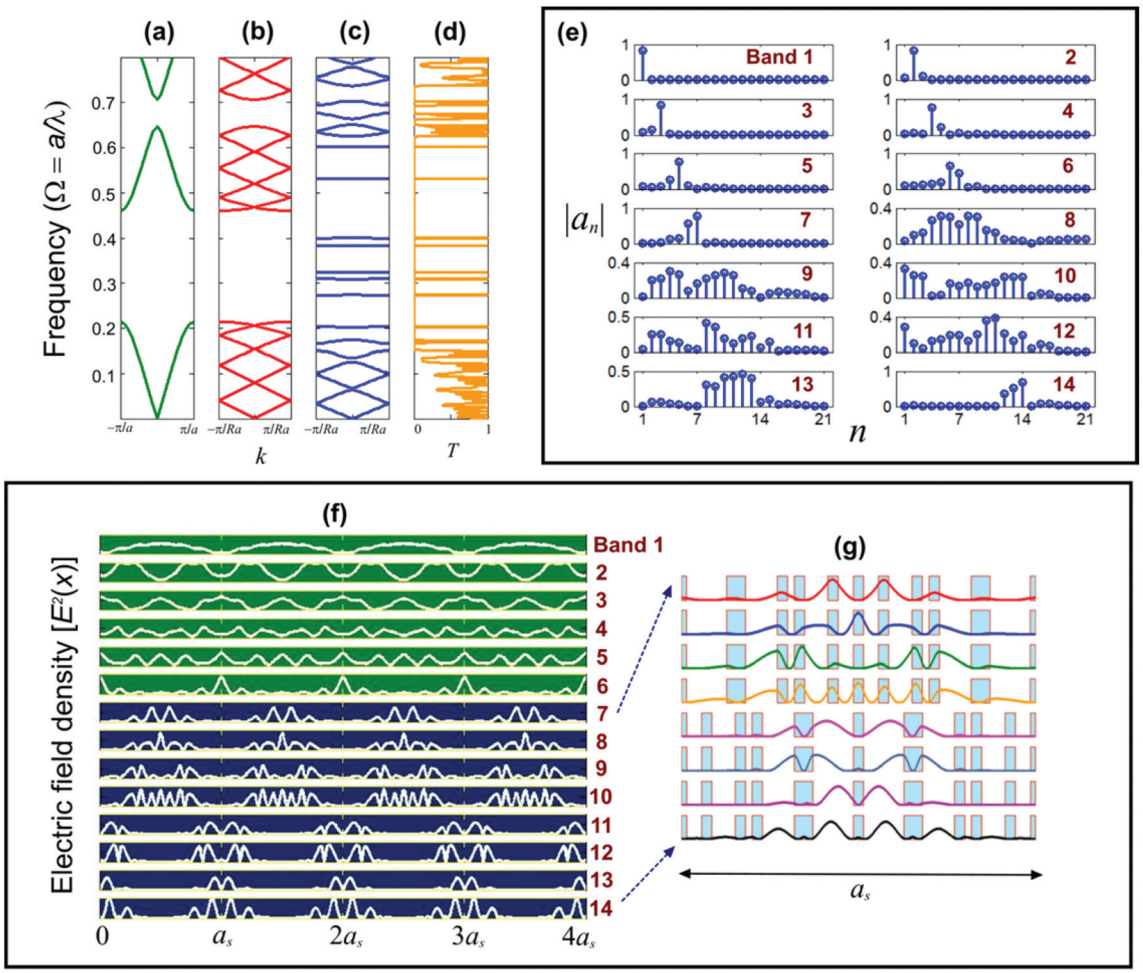

Fig. 2 (a) Band structure of PC1. (b) Folded band structure of PC1 for $R = 7$. (c) Band structure of the LCPC with $R = 7$. (d) Transmission spectrum of the LCPC with $R = 7$. (e) Bloch mode spectra for the LCPC modes ($R = 7$, $k = 0.2\pi/a_s$). (f) Mode profiles in the LCPC ($R = 7$, $k = 0.2\pi/a_s$). (g) Enlarged version of the mode profiles for bands 7–14 plotted within one period.

structures of LCPCs are very much different from the band structure of PC1, even though $r = R/(R-1)$ is close to 1. In the band structures of LCPCs, we can clearly see a specific frequency region $[0.18 < \Omega < 0.6]$ that houses the flat bands. For reasons that we shall explain, we name this region as the strong coupling region. As we can see from Fig. 3(a), the density of the flat bands in the strong coupling region increases as R increases (*i.e.*, r decreases towards one).

Let us understand the band structure of the LCPC in more detail, using the Bloch mode decomposition technique. The modes of PC1 are Bloch modes, and thus can be uniquely identified with their wavevectors. The Bloch modes with different wavevectors do not couple with each other, as long as the translational symmetry is conserved. When we combine PC1 with another PC that has a slightly different period, the original translational symmetry of PC1 is altered slowly, and this leads to a coupling of Bloch modes with different wavevectors.

The assessment of the mode coupling can be done by writing the dielectric function of the LCPC as $\varepsilon(x) = \varepsilon_1(x) + \varepsilon_p(x)$, where $\varepsilon_p(x) = \varepsilon(x) - \varepsilon_1(x)$ is the perturbation to the original dielectric function of PC1 $[\varepsilon_1(x)]$. The period of $\varepsilon_p(x)$ equals to the period of $\varepsilon(x)$, which is $a_s = Ra$. Since the period of the perturbing dielectric function $[\varepsilon_p(x)]$ is R times larger than the period of the unperturbed function $[\varepsilon_1(x)]$, the coupling between various modes of PC1 will take place only when the wavevectors of the modes differ by integer multiples of g. Therefore, it is instructive to consider a folded band structure of PC1. In the folded band structure, the original band structure of PC1 in the BZ of PC1 $[-\pi/a < k < \pi/a]$, is folded R times into the BZ of LCPC $[-\pi/(Ra) < k < \pi/(Ra)]$. In the folded band structure, the wavevectors of the neighbouring bands differ exactly by g. The folded band structure of PC1 with $R = 7$ is shown in Fig. 2(b). This band diagram is obtained by simply folding the bands in Fig. 2(a), 7 times into the BZ of the LCPC. Therefore, each original band in Fig. 2(a) becomes 7 folded bands in Fig. 2(b). These 7 folded bands touch each other at the edges, and along the same vertical line, the wavevectors of the neighbouring bands differ exactly by g.

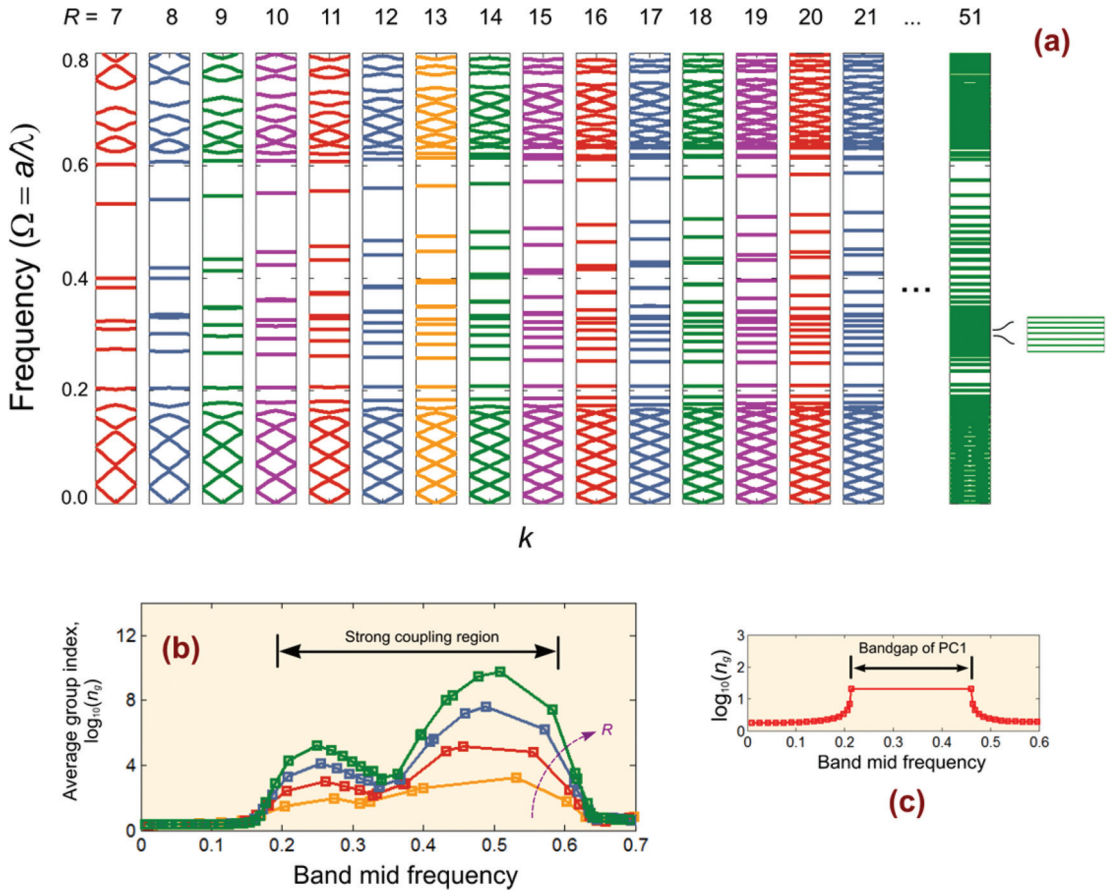

Fig. 3 (a) Band structures of the LCPCs for R = 7 to 51. (b) $\mathrm{Log}_{10}(n_g)$ as a function of the band mid frequency for the LCPC with R = 7, 11, 15 and 19. (c) $\mathrm{Log}_{10}(n_g)$ for the folded band structure of PC1 with R = 19.

When the perturbation $\varepsilon_p(x)$ is switched on, the folded bands of PC1 couple and interact with each other forming the band structure of LCPC as shown in Fig. 2(c). When we compare the folded band structure of PC1 [Fig. 2(b)], and the band structure of LCPC [Fig. 2(c)], we can see that in the long wavelength region (*i.e.*, $\Omega \ll 0.2$), the bands of LCPC are similar to the folded bands of PC1. Thus, the long wavelength region is a weak coupling region, as there is not much coupling between the folded bands of PC1. On the other hand, in the frequency region, $0.18 < \Omega < 0.6$, the band structures of LCPCs exhibit many flat bands [Fig. 2(c) and 3(a)]. These flat bands occur as a result of a strong coupling between the folded bands of PC1. Consistently, we name this frequency region as the strong coupling region.

We can quantify the Bloch mode coupling in the LCPC by expanding the electric field, $E(x)$, in the LCPC, as a linear combination of Bloch modes of PC1. Therefore, we have $E(x) = \sum_n a_n \phi_n(x)$, where $\phi_n(x)$ is the Bloch mode of PC1 corresponding to the n-th folded band, and a_n is the Bloch mode expansion coefficient. Using this expression for $E(x)$, we can transform the 1D time independent Maxwell equation into a linear eigenvalue problem. The coefficients a_n can then be extracted from the eigenvectors. The details of the eigenvalue problem are given in the ESI.†

Fig. 2(f) shows the electric field densities $[E^2(x)]$ for the first 14 bands of the LCPC with R = 7. The modes have $k = 0.2\pi/a_s$, and are plotted for 4 unit cells of the LCPC. The corresponding Bloch mode spectra ($|a_n|$ *versus* n plots) for these modes are shown in Fig. 2(e). From Fig. 2(e), we can see that the modes of the LCPC in the long wavelength region [for *e.g.* bands 1–3 in Fig. 2(c)] contain only one strong component of PC1's Bloch mode, whereas the modes corresponding to flatter bands (bands 7–14) are strong superpositions of many Bloch modes of PC1. Consistently, mode profiles [Fig. 2(f)] for the modes in the long wavelength region resemble those of a regular PC (*i.e.*, PC1). However, the modes corresponding to the flatter bands (which are strong mixtures of Bloch modes) are strongly localized within each unit cell of the LCPC [Fig. 2(f)]. The evanescent field of the localized mode from one unit cell is connected to the evanescent field of the identical localized mode in the adjacent unit cell. Evidently, this forms a chain of network that facilitates the propagation of slow light [Fig. 2(f)]. This is very much similar to the propagation of slow light in the typical coupled resonator optical waveguides.[22] In Fig. 2(g), we plot the enlarged versions of the mode profiles for the flat bands [bands 7–14], in one unit cell of the LCPC (R = 7). Notice that, the electric field densities for the bands 7–10 of the LCPC are concentrated in the dielectric regions at the

middle of the unit cells [see Fig. 2(f) and (g)]. The electric field densities for the higher frequency bands (bands 11–14) are concentrated in the air regions at the edge of the unit cells [notice the shifted unit cell in Fig. 2(g) for the bands 11–14].

What happens when R increases (*i.e.*, r reduces towards 1)? When R increases, the number of folded bands of PC1 increases. Consequently, a strong coupling and interaction between these folded bands leads to an increase in the number and density of the flat bands of LCPC [see Fig. 3(a)]. Apart from the increase in the density of flat bands, the bands also become flatter as R increases.

Let us analyse the flatness of bands in LCPC as a function of R, by defining an average group velocity, and an average group index. The average group velocity is defined as $v_g = \Delta\omega/\Delta k = c(2R\Delta\Omega)$, where $\Delta k = \pi/(Ra)$ is the length of half BZ, and $\Delta\Omega = |\Omega[k = 0] - \Omega[k = \pi/Ra]|$ is the frequency span of the band (*i.e.*, bandwidth). The average group index is then defined as $n_g = c/v_g = 1/(2R\Delta\Omega)$. As we can see from these expressions, v_g and n_g are directly related to the product $R\Delta\Omega$. Fig. 3(b) shows the $\log_{10}(n_g)$ *versus* band mid frequency plots for R = 7, 11, 15 and 19. In order to calculate n_g, we used band structures that are obtained from an exact formulation of the transfer matrix method, with a very high frequency resolution. As we can see from Fig. 3(b), in the long wavelength region, LCPCs of all R exhibit similar n_g. The value of n_g in this region can be well approximated using the effective refractive index formula, $\sqrt{\varepsilon_a F + \varepsilon_b(1-F)}$. Also from Fig. 3(b), regardless of R, we can clearly identify a region of frequencies ($0.18 < \Omega < 0.6$) in which the enhancement of n_g is very significant. This is the strong coupling region, in which modes of the LCPC occur as strong mixtures of Bloch modes of PC1. In the strong coupling region, as R increases, n_g of the flat bands increases significantly. From Fig. 3(b), we can see that n_g can be as high as $\sim 10^8$ when R = 15. We can get an even larger n_g by increasing R. For the purpose of comparison, we have also plotted $\log_{10}(n_g)$ *versus* band mid frequencies for the folded band structure of PC1 with R = 19 in Fig. 3(c). In PC1, the enhancement of n_g occurs only near the band edge [Fig. 3(c)]. However, in the LCPC the enhancement of n_g occurs for a broader spectrum (*i.e.*, in the strong coupling region) with a much higher magnitude. It is worth noting that, in all the plots shown in Fig. 3(b), there are troughs in the n_g distribution between $0.3 < \Omega < 0.4$. The troughs in the n_g distribution occur around the transition point, where the electric field concentration transits from the middle to the edge of the LCPC unit cell [see Fig. 2(f) and (g)]. Note that in Fig. 3, the frequency axis represents normalized frequencies. Therefore, the exact positions of the discrete flat bands depend on the choice of a. Further, if one finds the bands (or peaks in the transmission spectrum) are too close, a and R can be adjusted so that a good signal to noise ratio, and therefore high fidelity,[23] can be obtained.

When R increases, r decreases towards one, and the size of the super cell $a_s = Ra$ increases. The increase in a_s has two effects. Firstly, the density of the slow modes in the strong coupling region is increased. Secondly, the coupling of evanescent waves between the modes of the adjacent supercells is reduced. Therefore, as R increases, the width of the flat band ($\Delta\Omega$) decreases, and the average group index (n_g) increases [Fig. 3(b)].

The large number of slow modes is useful in creating broadband slow light applications in the digital telecommunication systems. An essential component of broadband digital telecommunication is the wavelength-division multiplexing (WDM) technology.[24] In a WDM based broadband network, to make use of the broad bandwidth, multiple data channels are multiplexed together in a single fiber. A single LCPC structure can provide slow light effect for all the data channels in the WDM network. The maximum bandwidth that an LCPC can support is equal to the length of the strong coupling region [*i.e.*, see Fig. 3(b)].

The positions of the strong coupling regions (and therefore the maximum bandwidth) remain the same for all R [see Fig. 3(a) and (b)]. This is due to the fact that the corresponding Fourier transforms of the LCPC's dielectric functions of all R with $d = 0.2a$ are similar [see Fig. 1(c) and (d)]. If one would like to alter the position and the length of the strong coupling region, then one has to play with the parameters (such as d, type of logical operation and refractive index contrast) that will alter the Fourier transform of the dielectric function.

The simplest method to fabricate the proposed LCPC is by means of a multilayer deposition. When we logically combine two 1D PCs with periods a and ra, using the logical OR operation, the minimum difference in adjacent layer thickness is simply the difference in the two periods, $t = a(r-1) = a/(R-1)$. The thickness t imposes a limit on r for practical realizations. To illustrate practical values of t, consider an implementation at the telecommunication wavelength, λ = 1550 nm. Using the normalized frequency of $\Omega = 0.5$ [near this Ω, we have a large n_g; see Fig. 3(b)], the period of PC1 is $a = \Omega\lambda$ = 775 nm. Therefore, for R = 21 and 51, we have $t \sim 15$ and 40 nm, respectively. 1D multilayer structures with such dimensions can be easily fabricated using matured techniques such as chemical vapor deposition or bias-target depositions.[25]

In conclusion, we have presented a new PC architecture that results from the logical combination of two 1D PCs of slightly different periods. The optical properties of the resulting logically combined PC are strikingly different from the individual PCs before the combination. In particular, the logically combined PC exhibits a region of frequencies, called the strong coupling region that has a high density of slow modes. The large number of slow modes is extremely useful in creating broadband slow light applications such as broadband rainbow trapping, and broadband optical buffers. Although, we have presented results for the logical "OR" operation with a silicon–air material system, the conclusion remains the same for all kinds of logical operations, and for any combination of dielectric materials, as long as the corresponding spatial Fourier decomposition of the LCPC's dielectric function comprises a mixture of two slightly different periodicities.

References

1 T. F. Krauss, *Nat. Photonics*, 2008, **2**, 448.
2 T. Baba, *Nat. Photonics*, 2008, **2**, 465.
3 J. B. Khurgin and R. S. Tucker, *Slow Light: Science and Applications*, CRC Press, Boca Raton, 2009.
4 Q. Gan, Z. Fu, Y. J. Ding and F. J. Bartoli, *Phys. Rev. Lett.*, 2008, **100**, 256803.
5 Q. Gan, Y. Gaoa, K. Wagnerc, D. Vezenovc, Y. J. Dinga and F. J. Bartolia, *Proc. Natl. Acad. Sci. U. S. A.*, 2011, **108**, 5169.
6 L. Chen, G. P. Wang, Q. Gan and F. J. Bartoli, *Appl. Phys. Lett.*, 2010, **97**, 153115.
7 J. Li, T. P. White, L. O'Faolain, A. G. Iglesias and T. F. Krauss, *Opt. Express*, 2008, **16**, 6227.
8 F. C. Leng, W. Y. Liang, B. Liu, T. Biao Wang and H. Z. Wang, *Opt. Express*, 2010, **18**, 5707.
9 H. Kurt and D. Yilmaz, *Appl. Phys. B*, 2013, **110**, 411.
10 T. F. Krauss, *J. Phys. D: Appl. Phys.*, 2007, **40**, 2666.
11 N. Gutman, W. H. Dupree, Y. Sun, A. A. Sukhorukov and C. M. Sterke, *Opt. Express*, 2012, **20**, 3519.
12 H. Hu, D. Ji, X. Zeng, K. Liu and Q. Gan, *Sci. Rep.*, 2013, **3**, 1249.
13 C. Wu, A. B. Khanikaev and G. Shvets, *Phys. Rev. Lett.*, 2011, **106**, 107403.
14 R. Shimada, T. Koda, T. Ueta and K. Ohtaka, *J. Appl. Phys.*, 2001, **90**, 3905.
15 A. G. Yamilov and M. F. Bertino, *Opt. Lett.*, 2007, **32**, 283.
16 A. G. Yamilov, M. R. Herrera and M. F. Bertino, *J. Opt. Soc. Am. B*, 2008, **25**, 599.
17 K. Sakoda, *Optical Properties of Photonic Crystals*, Springer, Berlin, 2001, ch. 2.
18 A. Yariv and P. Yeh, *Optical Waves in Crystals*, John Willey and Sons Inc., New Jersey, 2003.
19 J. B. Khurgin, *Adv. Opt. Photonics*, 2010, **2**, 287.
20 E. Feigenbaum, N. Kaminski and M. Orenstein, *Opt. Express*, 2009, **17**, 18934.
21 L. J. Wang, A. Kuzmich and A. Dogariu, *Nature*, 2000, **406**, 277.
22 A. Yariv, Y. Xu, R. K. Lee and A. Scherer, *Opt. Lett.*, 1999, **24**, 711.
23 Y. Zhu, M. Lee, M. A. Neifeld and D. J. Gauthier, *Opt. Express*, 2011, **19**, 687.
24 G. E. Keiser, *Opt. Fiber Technol.*, 1999, **5**, 3.
25 Y. Shen, *et al.*, *Science*, 2014, **343**, 1499.